



RESEARCH ARTICLE

10.1029/2023JG007403

Key Points:

- *Sphagnum* leaf area index seasonality—in situ and derived from Sentinel-2 (with the SL2P10 algorithm)
- *Sphagnum* vegetation index dynamics (chlorophyll activity, green chromatic coordinate, moisture soil index, normalized difference index) and *Sphagnum* gross primary production drivers
- Potential use of Sentinel-2 vegetation indices for *Sphagnum* mapping

Supporting Information:

Supporting Information may be found in the online version of this article.

Correspondence to:

R. Garisoain and L. Gandois,
raphael.garisoain@meteo.fr;
laure.gandois@toulouse-inp.fr



Citation:

Garisoain, R., Delire, C., Decharme, B., Ferrant, S., Granouillac, F., Payre-Suc, V., & Gandois, L. (2023). A study of dominant vegetation phenology in a *Sphagnum* mountain peatland using in situ and Sentinel-2 observations. *Journal of Geophysical Research: Biogeosciences*, 128, e2023JG007403. <https://doi.org/10.1029/2023JG007403>

Received 20 JAN 2023

Accepted 26 SEP 2023

A Study of Dominant Vegetation Phenology in a *Sphagnum* Mountain Peatland Using In Situ and Sentinel-2 Observations

Raphael Garisoain^{1,2} , Christine Delire¹ , Bertrand Decharme¹ , Sylvain Ferrant³ ,
 Franck Granouillac², Virginie Payre-Suc², and Laure Gandois²

¹CNRM, Météo-France, CNRS, Université de Toulouse, Toulouse, France, ²Laboratoire Ecologie Fonctionnelle et Environnement, CNRS, Université de Toulouse, Toulouse, France, ³Centre d'Etudes Spatiales de la Biosphère, CNRS, CNES, IRD, INRA, Université de Toulouse, Toulouse, France

Abstract Peatlands store more than a third of the global soil organic carbon stock. Bryophytes, more specifically *Sphagnum* mosses, play a major role in the carbon and water cycles of these ecosystems. There is a need to include *Sphagnum* mosses into Earth system models to better simulate the dynamics of peatlands in a changing environment. Leaf area index (LAI) is a key plant trait that characterizes the plant photosynthesizing capacity. Moreover, LAI is a variable calculated by land surface models used in climate models, allowing control of the exchange of matter and energy between vegetation and the environment. There is extremely little data on *Sphagnum* LAI and none on its seasonal change. We monitored *Sphagnum* mosses LAI phenology in a mountainous peatland site (altitude of 1,343 m) from June to December 2021 using two methods: 2D scans of monthly *Sphagnum* moss samples and analysis of Sentinel-2 images. LAI derived from field campaigns and the remote sensing approach show a strong seasonality, with high peak values reaching 10 and 7 m²·m⁻², respectively. The Sentinel-2 images were also used to derive common vegetation indices. The moisture soil index effectively discriminates *Sphagnum*-dominated areas in the peatland. Satellite-derived LAI of *Sphagnum* mosses is directly correlated to gross primary production monitored by gas exchange measurements ($R^2 = 0.83$) but also to physical drivers of the environment such as air temperature ($R^2 = 0.74$) or water table depth ($R^2 = 0.61$) over the 2017–2021 period. It is therefore highly suitable to investigate ecosystemic functions.

Plain Language Summary *Sphagnum* mosses are the main organisms inhabiting Northern Hemisphere peatlands. Peatlands play a major role in the evolution of the global carbon cycle over the long term. Numerical models of continental surfaces do not correctly model the functioning of peatlands. This study aims therefore at improving carbon cycle modeling by providing needed knowledge on *Sphagnum* phenology. Vegetation indices are used to monitor the development of vegetation over time. Here, vegetation indices are measured from the harvesting of *Sphagnum* on a Pyrenean peatland. These field indices are compared to vegetation indices acquired through satellite imagery. The two types of measurements show a marked seasonality of *Sphagnum*, with a rapid growth phase in June–July. The second part of the study highlights the links between environmental parameters (air temperature, water table height, and solar radiation), satellite vegetation indices, and *Sphagnum* photosynthesis, allowing us to understand the functioning of the ecosystem. Finally, the remote sensing method performs well at mapping *Sphagnum* mosses. This will be useful to study peatlands on larger scales, especially for still unknown or inaccessible peatland sites, as well as for the monitoring of these ecosystems in the context of climate change.

1. Introduction

Although peatlands represent only 3% of the emerged continental surfaces (Xu et al., 2018) they store around 25% of the organic carbon stock in soils (Hugelius et al., 2013; Yu, 2012). Northern peatlands have played a crucial role in regulating carbon and water cycles since the Last Glacial Interstadial (Holocene) (Loisel et al., 2014, 2017; Treat et al., 2019). Henceforth, subject to climate pressures, modifications of the carbon cycle of peatland ecosystems are expected (Chaudhary et al., 2017; Ferretto et al., 2019). Alpine peatlands are less studied and their functioning is poorly understood. They are generally smaller than boreal peatlands and more scattered (Pullens et al., 2016; Rosset et al., 2020). Nevertheless, their known surface tends to increase as they are discovered (Bao et al., 2015). Alpine *Sphagnum* peatlands share some of the characteristics of boreal *Sphagnum* ones; common vegetation, a short growing season, and are subject to rapid and significant climatic change (Millar et al., 2017;

© 2023 The Authors.

This is an open access article under the terms of the [Creative Commons Attribution-NonCommercial License](https://creativecommons.org/licenses/by-nc/4.0/), which permits use, distribution and reproduction in any medium, provided the original work is properly cited and is not used for commercial purposes.

van der Knaap et al., 2011). Thus, alpine peatlands appear as good proxies for boreal peatlands in the context of climate change and require attention in their own right.

Today, Earth system models do not correctly integrate carbon cycling in peatlands (Müller & Joos, 2020), limiting their ability to simulate the amount of carbon that may be released by soils in climate change conditions. Indeed, to date, peatlands are not represented in the climate models used in the Climate Model Intercomparison Project 6 (CMIP6) designed to inform the latest Intergovernmental Panel on Climate Change report. Thus, the major role played by peatlands in regulating the carbon cycle is omitted from climate and carbon cycle projections. However, the climate community is engaged in efforts to incorporate peatland dynamics and vegetation into land surface models, focusing mainly on boreal peatlands (Chaudhary et al., 2020). Also, there have been some attempts to model peatland dynamics using land surface models with output from the CMIP ensembles used as drivers, this could be a way forward (Chaudhary et al., 2022; Zhao & Zhuang, 2023). *Sphagnum* mosses have been identified as “ecosystem engineer” bryophytes, creating their favorable living conditions (Clymo & Hayward, 1982). Northern peatland organic matter is essentially composed of *Sphagnum* mosses (Hayward & Clymo, 1983; Loisel et al., 2017; Potila & Sarjala, 2004; Williams & Yavitt, 2003). Thus, modeling the functioning of *Sphagnum* in land surface models would be a key element in understanding the functioning of the global carbon cycle.

Land surface models characterize the total area of leaves of a given vegetation type, by the leaf area index (LAI) defined as the green leaf area per unit ground surface area (Asner et al., 2003). LAI regulates the exchanges between vegetation and the atmosphere, that is, matter and energy fluxes. Its seasonal evolution profoundly affects the carbon balance of plants and carbon inputs to the soil. In the specific case of *Sphagnum*, the LAI (or more generally, the shoot area index) is often a prescribed variable, not dynamic, and considered to have little seasonal evolution (Korrensalo et al., 2017; Riutta et al., 2007). To date, only two studies are focused on the LAI of *Sphagnum* and more generally of mosses: Bond-Lamberty and Gower (2007) and Niinemets and Tobias (2019) proposed experimental protocols for calculating the LAI of *Sphagnum* and mosses, respectively. Both studies use harvesting methods combined with image processing (photo or 2D-scan) to calculate projected leaf area (PLA). Bond-Lamberty and Gower (2007) find *Sphagnum* LAI of $3 \text{ m}^2\text{-m}^{-2}$ while Niinemets and Tobias (2019), with their very detailed method report values up to $30 \text{ m}^2\text{-m}^{-2}$ for mosses, much higher than before for bryophytes. This study also showed that the LAI would be the main trait characterizing the canopy. The LAI of moss canopies is expected to be in the very high range of plant LAI and thus appears as the key variable to investigate. On the other hand, the LAI of vascular plants, also present on peatlands, has been widely studied (Juutinen et al., 2017; Sonnentag et al., 2007; Wilson et al., 2007). Satellite or drone-derived (Räsänen et al., 2020) images can serve as a basis for determining the LAI of peatland vegetation by image processing. The resulting vegetation LAI is often very low, around $1 \text{ m}^2\text{-m}^{-2}$. As suggested by some authors (Juutinen et al., 2017), the LAI of *Sphagnum* mosses obtained by satellite measurements is underestimated compared to that obtained in the laboratory, questioning the resolution of the satellite images. Indeed, satellite products do not observe *Sphagnum* moss alone, but the mosaic of communities present on the surface of the peatland.

Sentinel-2 images with a resolution of 10 m have been available to the scientific community since 2016. The LAI product, associated with its quality index, is provided via the Sentinel Application Platform (SNAP) toolbox, calculated thanks to the Sentinel-2 Level 2 Prototype Processor (SL2P) algorithm developed by Weiss et al. (2020). This LAI is defined as half of the photosynthetically active area of the vegetation per unit of horizontal ground area. There are still very few studies aiming at evaluating the SNAP toolbox LAI on specific vegetation types. One of them carried out in an African semi-arid agricultural area highlights the correlation between LAI SNAP toolbox products and already existing global products such as MODIS or Proba-V. The comparison is more difficult to establish with in situ measurements (Kganyago et al., 2020). Field measurements correspond to “true LAI” measurements, whereas satellite measurements are “effective LAI” (LAI_e) measurements. The effective LAI assumes the hypothesis of a random distribution of leaves of the vegetation studied, which is not necessarily the case. The clumping index makes it possible to go from the true LAI to the effective LAI, taking into account the density of the vegetation and therefore any shading effects (Weiss et al., 2020). A recent study (Brown et al., 2021) focused on the validation of the SL2P algorithm, for calculating the LAI according to the Weiss et al. (2020) method shows good performance in the prediction of effective LAI_e. We also learn that these algorithms have been incorporated into the Google Earth Engine (GEE) application, thus facilitating the use of the algorithm via GEE without going through the SNAP software.

To our knowledge, Sentinel-2 images have not yet been used to determine peatland *Sphagnum* moss LAI and its seasonal development. Moreover, other vegetation indices can provide additional information on vegetation cycles as well as on the seasonality of physiological processes such as photosynthesis. Arroyo-Mora et al. (2018) suggested that the scientific community should do the long-term evaluation of biophysical vegetation indices from Sentinel-2.

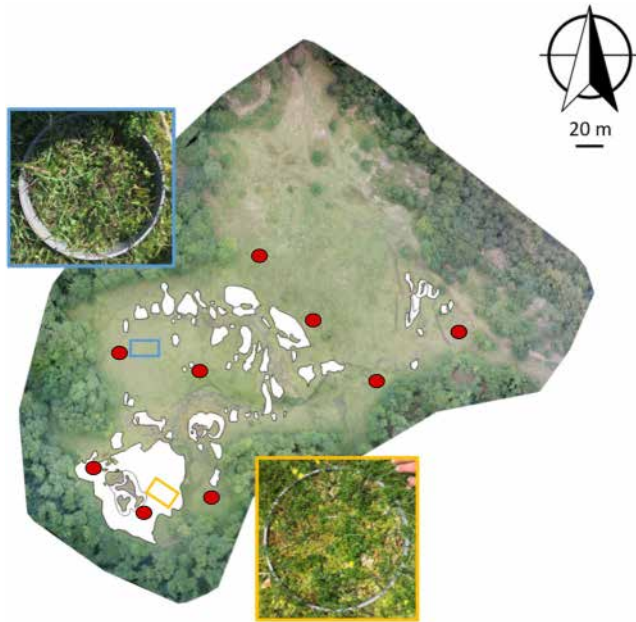


Figure 1. Aerial photograph of the Bernadouze peatland taken with a drone (Crédit: A. Séjourné). The white areas indicate the several *Sphagnum*-dominated areas from Henry et al. (2014). The two rectangles delimit the zones used for satellite-derived calculation: the orange for *Sphagnum* and the blue for herbaceous-dominated vegetation. The red dots correspond to the locations of the piezometers and soil collars. The two inserted photographs show bases where gross primary production fluxes are measured and illustrate the vegetation in the *Sphagnum*-dominated area (orange) and the herbaceous-dominated area (blue).

Usual indices such as normalized difference index (NDVI) or enhanced vegetation index have been studied and used to carry out environmental monitoring of *Sphagnum* peatlands. Although some studies highlighted their relevance (Lees et al., 2020), others pointed out their limitations (Pang et al., 2020). The main issue in peatlands is the difficulty to isolate the *Sphagnum* from the surrounding vegetation because of low satellite resolution (Harris et al., 2006). Although Harris (2008) highlighted the link between NDVI and *Sphagnum* photosynthetic activity, Lees et al. (2020), Letendre et al. (2008), and Tucker et al. (2022) showed that chlorophyll index (CI) (or modified CI) indices were better predictors of gross primary production (GPP) fluxes, although showing less sensitivity to the presence of *Sphagnum* compared to NDVI. Finally, Davidson et al. (2021) and Linkosalmi et al. (2022) emphasized the use of the green chromatic coordinate (GCC) to predict the GPP or maximum GPP on peatlands using phenocams and also Sentinel-2 derived GCC for the latter, but without focusing specifically on the presence of *Sphagnum*. Other indices described in the literature (photochemical reflectance index, green CI, modified CI) (Gitelson et al., 2005; Harris, 2008; Lees et al., 2020; Letendre et al., 2008) appear promising to predict *Sphagnum* photosynthetic activity, but cannot be calculated using the Sentinel-2 bands. To date, no study has yet established a link between *Sphagnum* GPP measured in the field and *Sphagnum* LAI derived from Sentinel-2 images at 10 m resolution.

This study is designed to investigate at the peatland scale, the fundamental biogeochemical and physical processes controlling the development of *Sphagnum* moss at a canopy level, using field and remote sensing approaches. This study has three main objectives. (a) Evaluation of the *Sphagnum* moss LAI and its seasonality, using laboratory scan and the first LAI satellite processing of the *Sphagnum* moss, (b) assessing the relevance of different satellite vegetation indices to detect the presence of *Sphagnum* and monitor their phenology in peatlands, (c) evaluation of the response of *Sphagnum* phenology and carbon assimilation to key abiotic factors of peatland functioning (air temperature, water table depth [WTD], and photosynthetic active radiation).

2. Materials and Methods

2.1. Study Site

The Bernadouze peatland is part of a national biological reserve, located at an altitude of 1,343 m in the eastern part of the French Pyrenees (42.80273°N; 1.42361°E). It covers an area of about 3.7 ha. The Bernadouze peatland is characteristic of alpine and southwestern Europe mountainous peatlands (Joosten et al., 2017). The peatland, receiving a continuous supply of water from precipitation and surface runoff (Joosten & Clarke, 2002) is classified as a soligenous fen. The peatland is surrounded by a beech forest that extends from the edge of the fen up to 1,800 m. The 10,000-year-old peatland has an average depth of 2 m, with some areas down to 10 m (Jalut et al., 1982; Reille, 1990). The current vegetation is mostly a fen, with 20 types of tracheophyte vegetation and 8 types of bryophyte vegetation (Henry et al., 2014). However, hummocks of *Sphagnum palustre* and *Sphagnum capillifolium*, reveal progressive ombrotrophic processes in some peatland areas (Erudel et al., 2017; Henry et al., 2014). The sampling zones are representative habitats of the peatland (Figure 1). The first one is at the South-West end of the peatland, where an important *Sphagnum* carpet has developed, mainly *Sphagnum palustre*, specifically through numerous *Sphagnum* mounds. This is the main ombrotrophic part of the peatland. It is also made of acidophilous turficulous species: *Molinia caerulea* subsp. *caerulea*, *Carex echinata* or *Viola palustris* mingling with the procession of larger species: *Carex nigra*, *Dactylorhiza maculata* or *Trichophorum cespitosum* subsp. *cespitosum*. Numerous small mounds dot the middle areas of the peatland and constitute stages of vegetation transition. They can be interpreted as localized phenomena of ombrotrophication where mainly *Sphagnum capillifolium* grows. The second sampling zone (Figure 1) is dominated by herbaceous plants. It is

part of a complex with a dull grass characterized by the abundance of *Molinia caerulea* subsp. *caerulea*, *Carex panicea* and *Carex nigra*.

2.2. Site Instrumentation

A weather station is located 350 m away, a little higher than the peatland, near a refuge (1,416 m). It is equipped with a thermometer, an automatic device measuring precipitation (snow + rain), snow depth, a wind sensor, and a radiation sensor at a frequency of 30 min (Gascoin & Fanise, 2018). Nine piezometers, spread out over the peatland, continuously record the WTD at an hourly frequency (Rosset et al., 2019). A radiation sensor measuring photosynthetically active radiation (PAR) is located in the middle of the peatland, recording data at an hourly time step (installed in 2018). The PAR data were not continuous due to battery failures. Thus, the S2M reanalysis time series was chosen for homogeneity. The S2M reanalysis is a combination of the SAFRAN meteorological reanalysis and the SURFEX/ISBA-crocus snow model cover (Vernay et al., 2022). The used reanalysis is a local mode application of the S2M chain, that is, at the scale of the “Couserans” massif. The weather conditions are considered homogeneous throughout the massif for the same altitude. The vertical resolution of the S2M model is 300 m, at hourly frequency. The topography of the place is taken into account through three parameters: the altitude, the slope, and the aspect of the site. A solar mask allows for taking into account the topography at the level of radiation and therefore takes into account the shading effects of the topography. The S2M channel provides a time series from 2017 to 2021 corresponding to direct and diffuse incident solar energy. We used a linear regression between the measured PAR radiation in the field and the total incident radiation from S2M to validate the PAR time series (slope of 2, $R^2 = 0.8$).

2.3. Field Sampling

Sphagnum samples were collected monthly from April to November (snow-free season) in 2021. For each sample, an area of 25 cm² (5 cm × 5 cm) was harvested using a square wire frame. Whole *Sphagnum* mosses were harvested by hand and stored in sealed plastic bags, all kept in an insulated bag for transport to the laboratory. Two types of *Sphagnum* have been identified corresponding to the main species present in the ombrotrophic areas of the peatland: *Sphagnum palustre* and *Sphagnum capillifolium* (Henry et al., 2014). Ten replicates were collected during each sampling campaign, covering one main area of approximately 40 × 60 m² (S-W end of the peatland) and others in the middle of the peatland (see Figure 1, white areas).

2.4. CO₂ Flux Measurements

Different measurements have also been carried out since 2016 during the monthly field campaigns close to the piezometers. Systematically and randomly, five out of the nine piezometer locations are chosen to carry out measurements of CO₂ flux (photosynthesis and respiration). The CO₂ fluxes are measured around noon with a portable transparent soil chamber (30 cm height, 30 cm diameter), fitted on fixed soil collars. The first measurement taken under natural light conditions gives the net ecosystem exchange (NEE) flux. The second measurement, using a dark chamber, captures the ecosystem respiration (ER), the sum of aboveground respiration (plants foliage) and belowground respiration (roots, soil organisms) (Janssens et al., 2001). Then, GPP (gross photosynthetic uptake) is deduced from the net flux and the ER (NEE = ER – GPP). The CO₂ concentration within the chamber headspace is monitored thanks to a CARBOCAP® GMP 343 CO₂ probe (VAISALA) placed at the top of the chamber for CO₂. Starting from 2019, a LI-COR LI-7810 analyzer was also connected to the chamber and used to measure CH₄ fluxes.

2.5. LAI From Field Sampling

Green LAI is calculated as the green surface area measured by a LI-COR 2D scanner divided by the sampling area (25 cm²). The LAI measured by the 2D scan (planimetric method) is a PLA (Bond-Lamberty & Gower, 2007; Jonckheere et al., 2004). According to Bond-Lamberty and Gower (2007), the PLA is related to the hemisurface leaf area (Chen & Black, 1992) by a factor of $\frac{\pi}{2}$ for *Sphagnum* $LAI = PLA \times \frac{\pi}{2}$. Here, we use this latter definition.

2.6. Satellite LAI Retrievals and Vegetation Index Calculation

We used remote sensing data (Copernicus Sentinel data) from the Sentinel-2 satellites to derive the evolution of LAI from 2017 to 2021, establish the reflectance spectrum of the peatland vegetation and calculate commonly used vegetation indices over the peatland. The two Sentinel-2 satellites carry a multi-spectral imager sensor providing a set of 13 spectral bands spanning from the visible (VIS) and near-infrared (NIR) to the shortwave

Table 1
Indices Used in This Study

Name	Reflectance equations	Bands equations	Resolution (m)	Purpose	Reference
NDVI					
Normalized difference vegetation index	$\frac{R_{850} - R_{680}}{R_{850} + R_{680}}$	$\frac{B8 - B4}{B8 + B4}$	10	Vegetation index	Rouse et al. (1974)
MSI					
Moisture soil index	$\frac{R_{1550} - 1750}{R_{760} - 800}$	$\frac{B11}{B5}$	20	Moisture index	Vogelmann and Rock (1986)
GCC					
Green chromatic coordinate	$\frac{R_{green}}{R_{green} + R_{blue} + R_{red}}$	$\frac{B3}{B2 + B3 + B4}$	10	Greenness index	Richardson et al. (2007)
CI					
Chlorophyll index	$\frac{R_{750}}{R_{705}} - 1$	$\frac{B6}{B5} - 1$	20	Chlorophyll index	Gitelson and Merzlyak (1994)

infrared (SWIR) (443–2,190 nm). Four bands have a spatial resolution of 10 m (VIS and NIR bands), six bands of 20 m (red-edge and SWIR), and three bands at resolution of 60 m. Snow cover periods have not been covered. The annual cycles presented, therefore, go from April to November (included).

The LAIs were calculated using the LEAF toolbox developed by Fernandes et al. (2021). The LEAF toolbox is an open-source application, available on GEE, and allows to perform various Level 2 Vegetation Biophysical Products processing. LEAF is a better implementation of the SL2P algorithm (Weiss et al., 2020). Indeed, the SNAP (ESA's SNAP) “Biophysical Processor” had an incorrect implementation of the sampling used to define the calibration database (<https://github.com/rfernand387/LEAF-Toolbox/wiki/FAQ>). Here, the python API was used to run the SL2P algorithm at 10 m resolution to calculate LAIs at 10 m resolution. The primary purpose of this tool is to generate LAI maps on regions of interest but not time series, we slightly modified the available python API to calculate the LAI on the Bernadouze area over the 2017–2021 period. The biophysical processor determines the LAI using a set of backpropagation artificial neural networks (ANNs) trained by worldwide distributed simulations from a radiative transfer model (PROSAIL, <http://teledetection.ipgp.jussieu.fr/prosail>). The ANN requires as inputs: reflectance bands (B3–B7, B8a, B11, and B12) and viewing zenith, solar zenith, and relative azimuth angles characterizing the satellite orbit (Weiss et al., 2020). Here, the Sentinel-2 S2-SR (Sentinel-2 reflectance) harmonized images data set was used as input.

We computed commonly used vegetation indices (see Table 1) sensible to vegetation activity (NDVI), vegetation greenness (GCC), CI, and vegetation moisture content (MSI). The vegetation indices were calculated thanks to the use of the GEE code editor, with the S2-SR harmonized images data set. S2 SR harmonized data set is available on GEE, and provides atmospherically corrected surface reflectance images. A filter of clouds at 30% on the peatland area has been applied to all the data (LAI and vegetation indices). Due to the presence of snow from November to February, LAI and indices have not been calculated over these months. After removing the cloudy images, we were able to use an average of four images per month, or approximately one image every 7 days. The months of June–August often benefit from more favorable atmospheric conditions, with clear skies, allowing us to exploit an average of six images per month for the latter. Considering only snow-free and cloud-free images, we obtained a data set of 202 images over 5 years. LAIs and vegetation indices were then averaged over two areas of 20 m × 15 m, one dominated by *Sphagnum* moss (orange area in Figure 1), and the other one by herbaceous plants (blue area in Figure 1).

Finally, linear interpolations were applied to vegetation indices and LAI data to obtain time series of daily data. The mean annual cycle of daily LAI (and vegetation indices) was then calculated from the interpolated signals over the period 2017–2021.

2.7. Vegetation Index Maps

We produced maps of the CI, GCC, NDVI, and MSI and compared them to a reference vegetation map to test the ability of the indices at detecting *Sphagnum*. We chose the date of the maximum GCC of the year 2021 (21 July) to produce the vegetation index maps and facilitate detection. The maps were generated with GEE. The vegetation index maps were normalized so that the indices varied from 0 to 1 on the entire peatland and the different indices

maps could be compared. The maximum and minimum values of the vegetation indices on the peatland before normalization range for the CI from 0 to 3.5, the GCC from 0.3 to 0.6, the MSI from 0.3 to 2, the NDVI from 0.1 to 1. The vegetation index maps were compared to a reference vegetation map by calculating Pearson's correlation coefficients. Henry et al. (2014) had made a fine georeferenced vegetation map of the peatland at a resolution of 4 m, by observation and photography. With this botanical map, we constructed the reference map, simply by identifying the presence or absence of *Sphagnum* mosses in the vegetation groups from Henry et al. (2014) (Figure S1 in Supporting Information S1). This new reference map was then re-sampled at 10 m resolution. Confidence interval at 95% of Pearson coefficients were estimated thanks to the bootstrap function of the `scipy.stats` library which allow to “Compute a two-sided bootstrap confidence interval of a statistic.” (<https://docs.scipy.org/doc/scipy/reference/generated/scipy.stats.bootstrap.html>)

2.8. Reflectance Spectra

We calculated the reflectance spectra of *Sphagnum* using the SNAP toolbox. We used an image acquired on 21 July 2021, at a time when *Sphagnum* growth was high. The image was downloaded from the ESA PEPS platform (<https://peps.cnes.fr>). It is an L1C top-of-the-atmosphere product. An atmospheric correction was then applied to the L1C product, using the ESA Sen2Cor module, to obtain the L2A top of the canopy product. We then chose a “subset” of the image, corresponding to the Bernadouze peatland, and resampled the spectral bands (B3–B7, B8a, B11, B12) at a resolution of 10 m. The same two distinct vegetation zones as above were selected to plot the spectrum (orange and blue areas in Figure 1).

2.9. Time Series and Statistical Analysis

To make statistical analyses, we first built daily time series. The hourly WTD measurements from the nine piezometers were averaged out to get one daily time series. The daily time series of PAR was built using only values between 11 and 13 local time to coincide with the timing of the CO₂ flux measurements. We then calculated the mean annual cycle of WTD and PAR over the 2017–2021 period and applied a 10-day rolling mean to smooth out the signal. For the GPP flux, to compensate for the small number of data per year (once a month), we used the measurements from the 5 years to build one annual cycle. We then applied a B-spline function (degree 3) to obtain a time series of daily midday GPP values. We obtained an annual cycle including the 5 years. Finally, the Pearson correlation coefficient was evaluated over all the annual cycles in a correlation matrix (not shown here).

3. Results

3.1. LAI: 2D Scanner Versus Satellite-Derived Values

We find that *Sphagnum* LAI derived from both the 2D-scanning and the remote sensing approach show a strong seasonality from June to December 2021 with high peak values (Figure 2). *Sphagnum* LAI from 2D scans varies from 3.5 to 10 m²·m⁻². The maximum is reached in August. The LAI of the *Sphagnum*-dominated area, derived from Sentinel-2 varies from 0.5 to 7 m²·m⁻², with a maximum value reached in July. In the herbaceous plant-dominated area, the LAI from Sentinel-2 varies from 0.5 to 5 m²·m⁻², with a maximum reached in July. Herbaceous and *Sphagnum* Sentinel-2 LAI share the same seasonality. The peak of 2D-scan LAIs is shifted in August compared to the one obtained with Sentinel-2 processing. Here and in the rest of the document remotely sensed derived LAI (or indices) of the *Sphagnum*/herbaceous dominated area will be named satellite *Sphagnum*/herbaceous LAI (indices). For 2D scan LAI, and GPP or other measurements made on the peatland we use the term ground LAI, GPP.

3.2. Satellite Reflectance Spectra Analyses

The reflectance spectral signature of *Sphagnum* moss stands out from that of other types of vegetation. The characteristic green peak (560 nm) is visible, as well as the peak at 842 nm in the near-infrared as already described by Harris et al. (2006), Pang et al. (2020), or Erudel et al. (2017) at a better resolution. From 400 to 900 nm, the spectrum of the *Sphagnum* zone is higher than that of herbaceous plants. After 900 nm, advancing in the SWIR domain, the *Sphagnum* spectrum decreases and merges with that of the herbaceous vegetation until it falls below the herbaceous spectrum, with a maximum difference between the two spectra at band 11. In the visible, the reflectance spectrum of the *Sphagnum* zone is higher, reflecting the lower capacity of *Sphagnum* to absorb PAR radiation. According to Figure 3, bands around 850 nm like band B8 or also bands B6 and B7 appear interesting to discriminate *Sphagnum* from herbaceous plants. However, many herbaceous

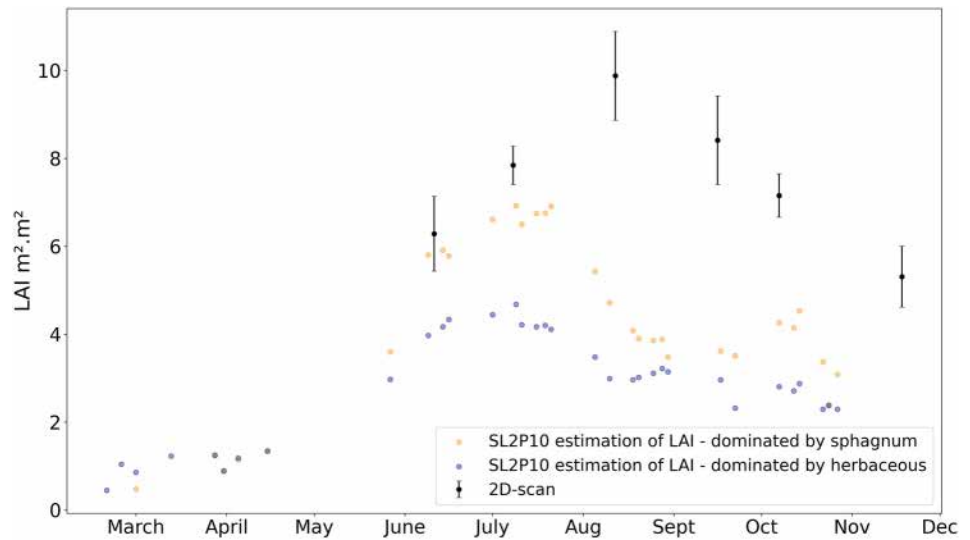


Figure 2. Seasonal development of the leaf area index (LAI) over the year 2021. The black dots are the 2D scans (collected in the *Sphagnum*-dominated area). In colors, satellite SL2P10 estimated LAI of the *Sphagnum*-dominated area (orange) and the herbaceous plants-dominated area (blue). The vertical bars correspond to the 95% confidence interval of the spatial uncertainty ($n = 10$, covering $40 \times 60 \text{ m}^2$).

plants show high reflectance values between 750 and 850 nm on the Bernadouze peatland (not shown), just like *Sphagnum*. These hypothesis and other indices were tested and then discarded. Instead, we used the ratio of bands B11 (1,610 nm) and B5 (705 nm) to discriminate *Sphagnum* from the surrounding vegetation. Indeed, the ratio of the reflectances of these two bands is smaller for the *Sphagnum* zone compared to the herbaceous one. The spectrum was calculated on other herbaceous areas, and the ratio of B11 and B5 always remains the smallest in places with *Sphagnum* (not shown here). This ratio corresponds to the MSI (see Table 1).

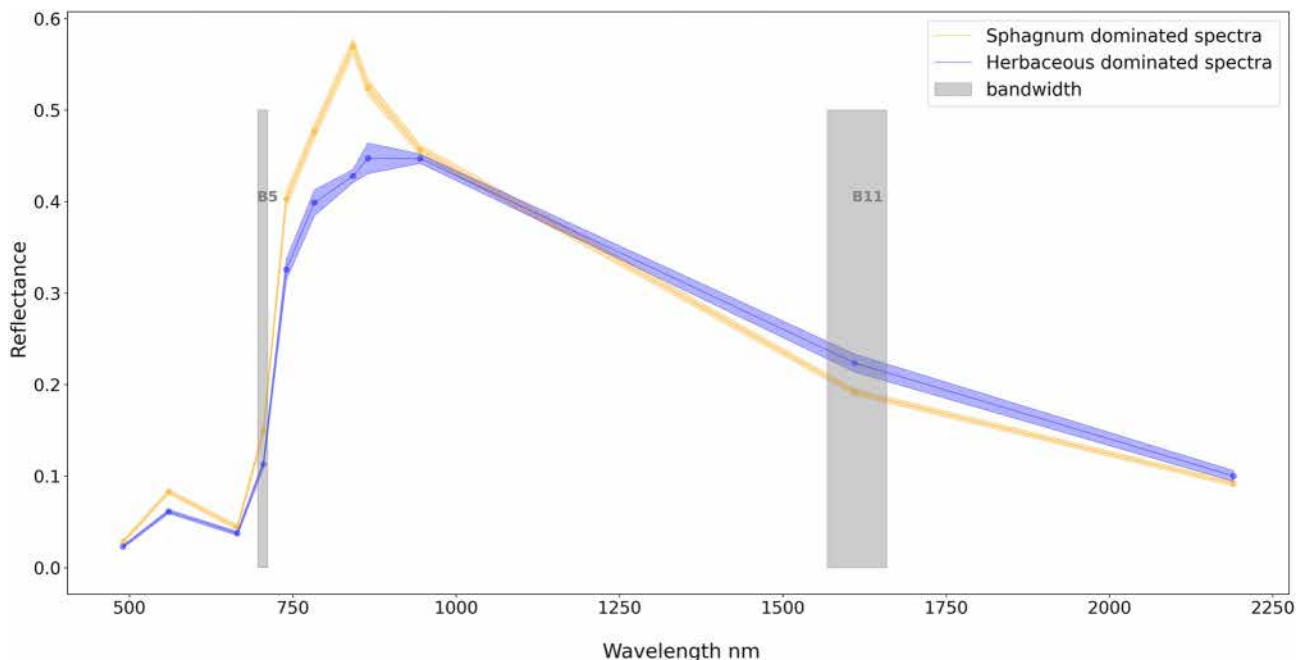


Figure 3. Mean reflectance spectra of Sentinel-2 instruments for the *Sphagnum*-dominated (yellow) and herbaceous-dominated areas (blue) on the 21 July 2021. In lighter hue are the 95% confidence intervals to the mean. B5 and B11 bands are highlighted in gray.

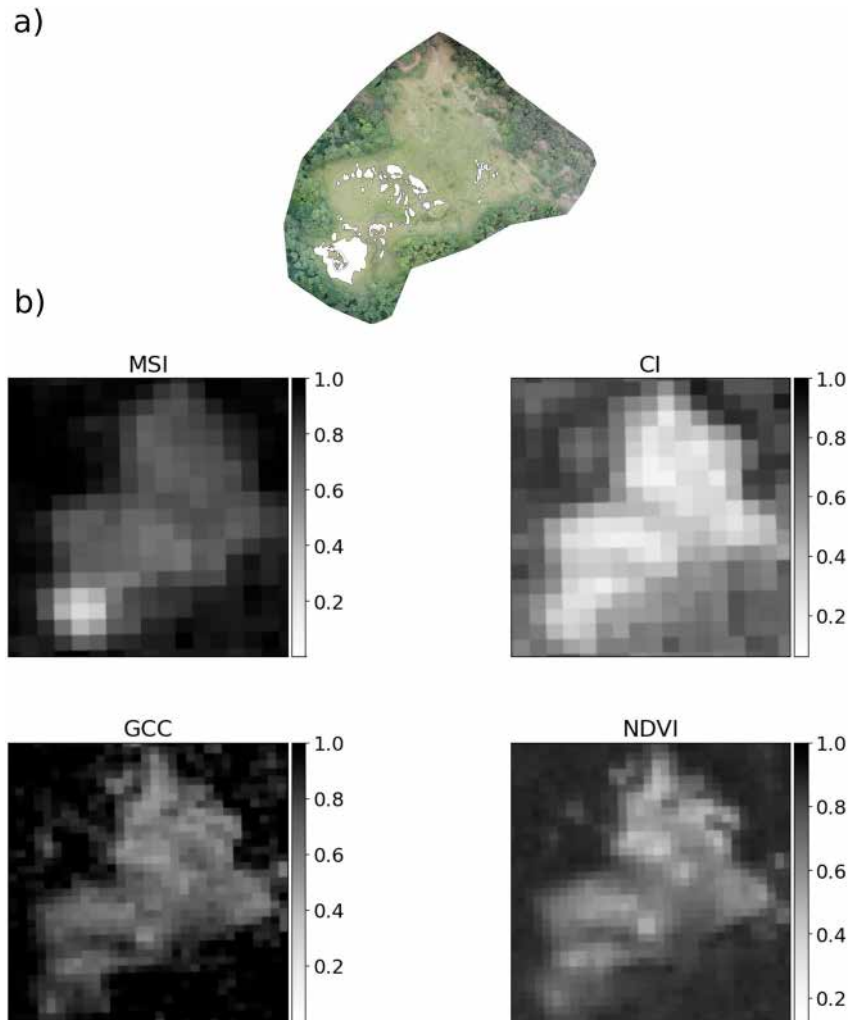


Figure 4. (a) The location of *Sphagnum* mosses (white areas) superimposed on the aerial photograph of the site from Figure 1 for comparison. (b) Maps of moisture soil index (MSI), chlorophyll index (CI), green chromatic coordinate (GCC), and normalized difference index (NDVI) over the Bernadouze peatland on 21 July 2021. MSI, NDVI, CI, and GCC maps were normalized following $\frac{X-X_{\min}}{X_{\max}-X_{\min}}$, with X the pixel values of the considered index, X_{\min} , X_{\max} respectively the minimum and the maximum pixel value of the considered index in each map.

3.3. *Sphagnum* Detection With Vegetation Indices

Figure 4 illustrates the difference between the four spatialized indices (MSI, GCC, CI, and NDVI) on the peatland. The *Sphagnum* zone is clearly identified thanks to the MSI unlike other indices and in line with our analysis of the spectral properties of *Sphagnum* (Section 3.2). See Pearson coefficients in supporting information for quantitative explanations and comparison with a reference vegetation map of the peatland. The zone where *Sphagnum* is dominant corresponds to the lowest MSI values (lighter gray and white). The *Sphagnum* zones have high GCC and NDVI (darker gray) but these values cannot be distinguished from the N-E limit of the meadow that is mostly rocky and does not have any *Sphagnum* or to other darker gray pixels in the images corresponding to areas without *Sphagnum*. The CI does not allow to distinguish *Sphagnum* mosses.

3.4. Seasonality of the Peatland as Seen by Satellite-Derived Vegetation Indices and Vegetation Productivity in Comparison to the Seasonal Cycles of Air Temperature, Photosynthetic Active Radiation and Water Table Depth

The temporal evolution of the vegetation indices Figure 5 reveals two groups: the GCC, CI, and satellite LAI for the first and NDVI and MSI for the second. The seasonal cycles of satellite LAI, GCC, and CI indices are in phase and

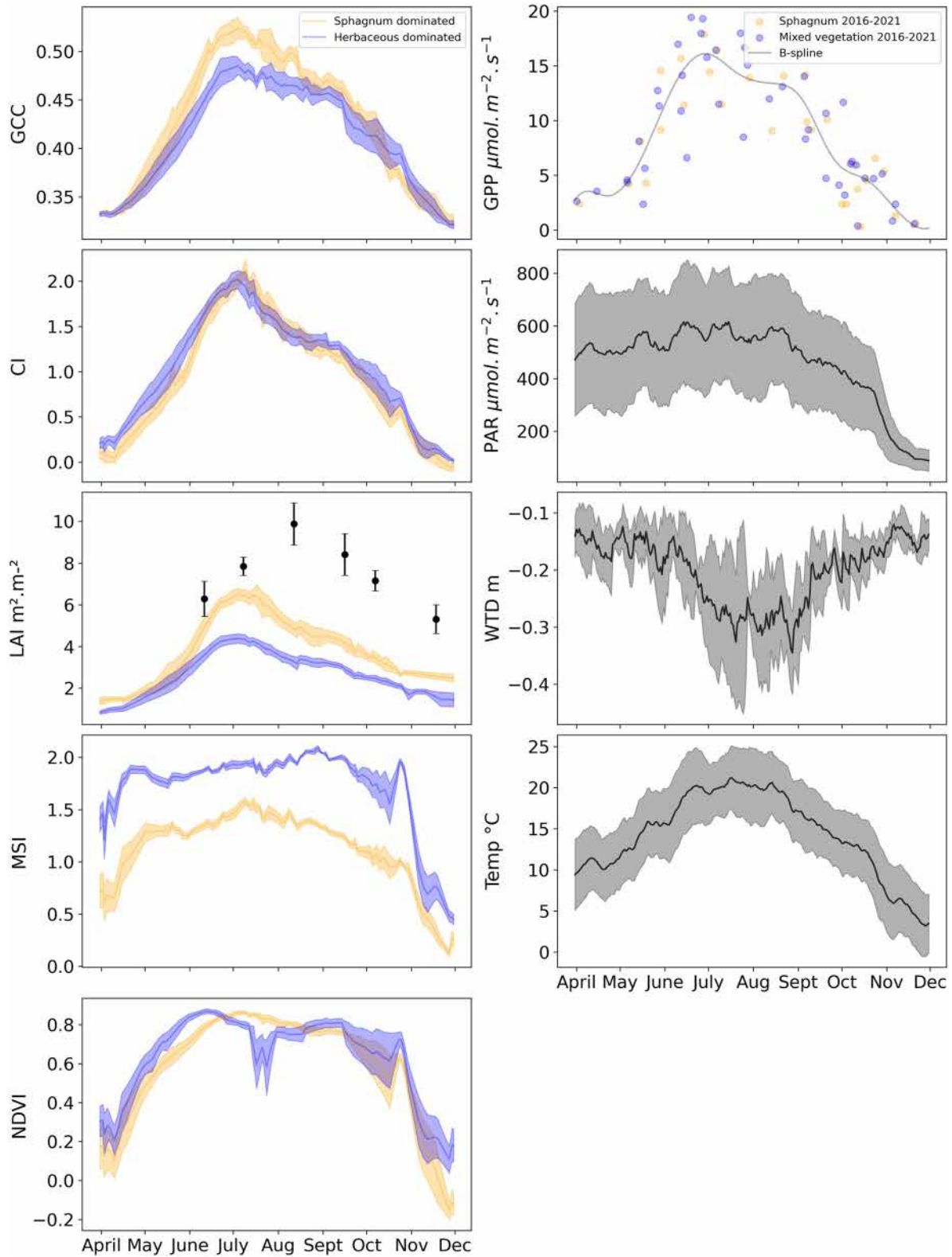


Figure 5. Green chromatic coordinate (GCC), chlorophyll index (CI), satellite leaf area index (LAI), normalized difference index (NDVI), moisture soil index (MSI), gross primary productivity (GPP), photosynthetic active radiation (PAR), water table depth (WTD), air temperature (Temp) mean annual cycles and interannual variability from years 2017–2021 for the *Sphagnum* (orange) and herbaceous (blue) dominated areas at Bernadouze. The bands in lighter hue show the interannual variability (95% confidence interval). Ground LAI for the year 2021 is shown for reference (black dots with bars).

strongly correlated. They show a strong increase at the beginning of the season from April to mid-June and reach their peak at the end of July. Their decrease until the winter season is slower. NDVI and MSI show a fast increase from April to early June (May for MSI), then remain close to their maximum value until autumn when they decrease.

If there is almost no distinction between the *Sphagnum* and herbaceous-dominated areas for CI, the satellite LAI and GCC values are higher for the *Sphagnum*-dominated zone compared to the herbaceous-dominated zone, from June to November. At the start of the season, from April to May, the CI values for the *Sphagnum* zone are lower than those for the herbaceous area, indicating a lower photosynthetic activity of *Sphagnum*. For satellite LAI and GCC, it is the opposite. The rapid and significant evolution of the LAI of *Sphagnum* allows the photosynthetic activity of *Sphagnum* to catch up with that of herbaceous plants from the month of June, to then evolve in a joint manner. *Sphagnum* therefore seems to react and develop more quickly than herbaceous plants, as soon as the growing conditions are favorable to them. Although *Sphagnum* mosses have a lower photosynthetic capacity than herbaceous plants, this is compensated by higher LAI. The LAI of *Sphagnum* mosses, from its maximum, decreases less rapidly than that of herbaceous plants.

The seasonal variation of the *Sphagnum* and herbaceous dominated zones GPPs from our ground measurements are within each other interannual variability (Figure 5 and Figure S2 in Supporting Information S1), unlike the satellite-derived LAI or GCC index. The GPP presents a similar evolution as CI, GCC, and LAI (Figure 5), that is, a marked increase at the start of the season up to a maximum at the end of June-beginning of July before slowly decreasing. The correlations between GCC, CI, LAI, and GPP annual cycles are also very strong ($R^2 = 0.94, 0.94, 0.83$, respectively).

The annual cycles of NDVI and MSI, are more difficult to interpret and link to the functioning of the peatland. The long plateaus in summer point to a saturation of the indices. However, the large difference in the MSI values of *Sphagnum* and herbaceous plants from April to October confirms that MSI is a good tool to detect *Sphagnum*-dominated areas during the whole growing season.

On average, PAR varies very little from April to August (Figure 5), during the growing phase of the vegetation. This means that on average, there is enough light for vegetation growth on the peatland from April to August and that PAR is not a limiting factor during these months. From September on, PAR decreases strongly, which is coherent with the decrease in GPP and vegetation indices.

The WTD has on average a reversed seasonal cycle compared to GPP and the vegetation indices (Figure 5). The water table remains close to the surface from April through June, decreases in summer and slowly increases from September to November. This anticorrelated seasonal cycle does not mean that vegetation productivity is favored by a low water table, but that the water table level in summer on average from 2017 to 2021 does not impede vegetation productivity.

The seasonal cycle of surface air temperature is highly correlated with the seasonal cycles of LAI, GPP and the other indices (Figure 6). This is particularly true from April to early July and suggests that the vegetation productivity and growth are driven by air temperature during this time of year. Air temperature remains stable in July and August, while LAI and GPP tend to slowly decrease, indicating that other factors are likely at play: a lower water table and slightly less PAR. The decrease in air temperature from September to December is in phase with the decreasing vegetation productivity and LAI but also with the decreasing PAR, indicating that both air temperature and PAR are likely responsible for the vegetation senescence.

The scatter plots of the LAI and vegetation indices versus surface air temperature, PAR, and WTD (Figure 6) highlight hysteresis cycles indicating the non-reversibility of the biophysical processes. The different behavior between the growing vegetation phase (dark brown to dark gray) and the senescence phase in autumn (light green to brown) is particularly obvious for air temperature (first column). The R^2 confirms the analysis of Figure 5:

1. The highest R^2 is found between surface air temperature and LAI, GPP, and vegetation indices, with the exception of MSI, confirming that air temperature is a major driver of vegetation growth and productivity. MSI is an indicator of vegetation moisture content, its weaker relation with temperature is expected.
2. The R^2 between LAI, GPP, CI, GCC, NDVI, and PAR are much lower, and reflect the different relation from April to July when PAR is fairly stable around $500 \mu\text{mol}\cdot\text{m}^{-2}\cdot\text{s}^{-1}$, and after, when PAR declines together with vegetation productivity and LAI.

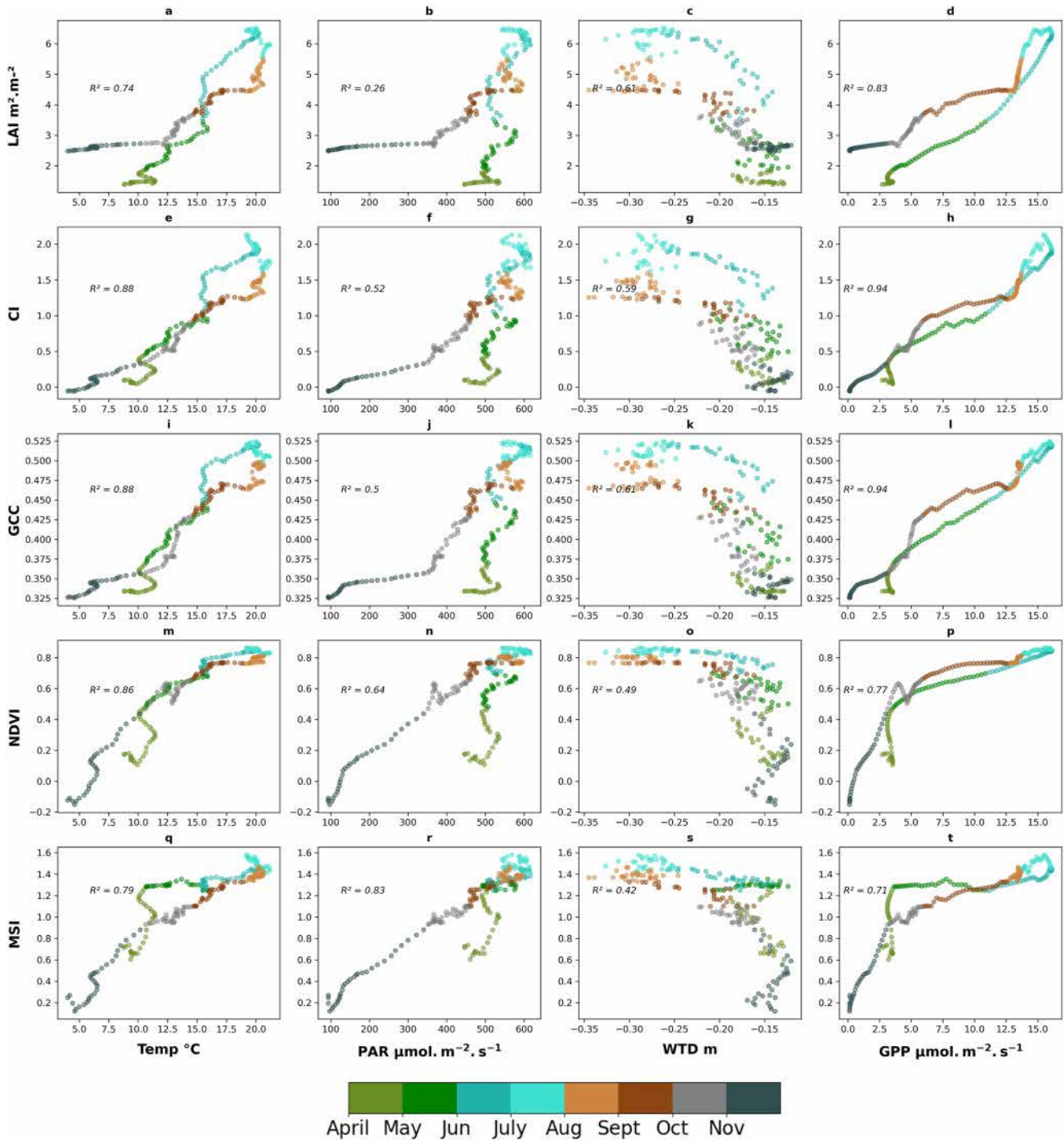


Figure 6. Scatter plots and R^2 of mean annual cycle of satellite leaf area index (LAI) ($\text{m}^2\cdot\text{m}^{-2}$), chlorophyll index (CI), green chromatic coordinate (GCC), normalized difference index (NDVI), moisture soil index (MSI) of the *Sphagnum*-dominated area against mean water table depth (WTD) (m), photosynthesis active radiation (PAR) ($\mu\text{mol}\cdot\text{m}^{-2}\cdot\text{s}^{-1}$), temperature (Temp) ($^{\circ}\text{C}$), growth primary productivity (GPP) ($\mu\text{mol}\cdot\text{m}^{-2}\cdot\text{s}^{-1}$) over 2017–2021.

3. The R^2 between the vegetation variables and WTD is also fairly low, and the scatter plots roughly show two behaviors, one when the water table is high (above roughly 22 cm) and when the water table drops below 22 cm.

Although LAI and GPP have a roughly similar seasonal cycle, the scatter plot of LAI versus GPP reveals that their seasonal cycles are not completely in phase. At the start of the growing season (light green), LAI ($<1 \text{ m}^2\cdot\text{m}^{-2}$), and

GPP ($3 \mu\text{mol}\cdot\text{m}^{-2}\cdot\text{s}^{-1}$) are low (Figure 6, last column). Then LAI and GPP increase almost linearly, until end of June when GPP reaches its maximum ($18\mu\text{mol}\cdot\text{m}^{-2}\cdot\text{s}^{-1}$). GPP then starts to decrease rapidly, while LAI remains around its maximum value ($6 \text{ m}^2\cdot\text{m}^{-2}$) until mid-July. LAI decreases sharply in August, while GPP remains fairly stable (light brown). From September to December, GPP decreases to zero while LAI only decreases to 2.5 (dark brown to dark gray, last measurements before snowfall). This different behavior in spring and autumn is most obvious in LAI versus GPP and exists to a lesser extent between GPP and the vegetation indices (Figures 6d, 6h, 6l, 6p, and 6t). The CI and GCC indices are linked with a linear relationship with GPP. The NDVI and MSI indices follow nonlinear relationships with GPP and saturate very quickly as soon as GPP increases to around $12 \mu\text{mol}\cdot\text{m}^{-2}\cdot\text{s}^{-1}$ (Figures 6p and 6t). The LAI, CI, and GCC indices have a more linear behavior with GPP as shown by the higher correlation coefficients.

4. Discussion

4.1. Potential and Limitations of the Use of MSI Index for *Sphagnum* Peatland Survey

We showed that the reflectance spectrum of *Sphagnum* moss measured with Sentinel-2 bands is different from the one of herbaceous vegetation. This opens the path toward the definition of specific *Sphagnum* indices that could be used for *Sphagnum* peatland detection and mapping. These remote sensing observations are coherent with in situ investigations using mobile spectroradiometers at higher resolution by Erudel et al. (2017), Harris et al. (2006), and Pang et al. (2020) who showed that *Sphagnum* mosses have a different spectral signature than vascular plants and other types of mosses. This is due to the combination of two factors: the network architecture of hyaline cells and chloroplasts and the high water retention capacity of *Sphagnum* (Pang et al., 2020). This results in a singular spectrum for *Sphagnum* in the NIR (near-infrared: 700–900 nm) and in the SWIR (shortwave infrared: 900–2,500 nm), respectively. The MSI index can be used to discriminate *Sphagnum* from the surrounding vegetation throughout the year, as shown in Figure 5. However, vegetation indices generally follow the evolution of ground vegetation density over time, which means that the indices increase when vegetation develops. This is not the case for the MSI index, because of strong interactions with water content. The 1,600 nm band is sensitive to the presence of water in the vegetation, unlike the near-infrared bands (Harris et al., 2006). The 1,600 nm reflectance band and the MSI are known to increase when plant water content decreases. This was observed at our site during a drought in 2019 when MSI greatly increased (Figures S3 and S4 in Supporting Information S1) due to the very dry conditions and not to an increased vegetation density, as already found by Meingast et al. (2014). Despite this limitation, the MSI is an effective index to discriminate *Sphagnum* carpets from the surrounding vegetation, taking care to avoid drought situations. Combined with a vegetation index in the visible, or a color segmentation algorithm in the visible, the MSI could be used in the detection of *Sphagnum* peatlands at a larger scale, especially in open and isolated mountainous areas where peatlands are often not yet identified. This would constitute a first step in the establishment of a more complete mapping of peatlands, taking into account the many peatlands still unidentified (Minasny et al., 2019).

4.2. Measurement of *Sphagnum* LAI Reveals a Strong Seasonal Pattern and High Peak Values

In this study, we showed a strong seasonal cycle of *Sphagnum* LAI. This will have a strong impact on the modeling of energy, water, and carbon cycle of peatlands at a global scale. Indeed, the leaf or shoot area determines the area that exchanges energy, water, and carbon with the soil and atmosphere and until now, when taken into account, peatland mosses are supposed to have a very low LAI, close to 1, with little seasonal variation (Drueel et al., 2017; Juutinen et al., 2017; Riutta et al., 2007). In other studies, moss phenology is either neglected or assimilated to that of herbaceous plants (Shi et al., 2021; Wania et al., 2009).

Our ground-measured *Sphagnum* LAIs reach higher values (around $10 \text{ m}^2\cdot\text{m}^{-2}$) than the satellite-derived ones ($7 \text{ m}^2\cdot\text{m}^{-2}$). This is coherent with Juutinen et al. (2017) who pointed out that the LAI values of *Sphagnum* moss were often underestimated by satellite products (Juutinen et al., 2017), because herbaceous and small shrubs coexist with *Sphagnum* in the zone studied. This might explain the observed discrepancy between the peak of *Sphagnum* moss LAI estimated by satellite and by 2D scans. This is an illustration of the “signal averaging” effect already described by Harris et al. (2006). Thus, assuming a nonnegligible contribution to the reflectance signal from herbaceous plants, this would therefore tend to lower the average satellite value of the *Sphagnum*-dominated area. It can be expected that true *Sphagnum* LAI are greater than those obtained using the satellite product.

Then, the observed ground LAI (2D scan) is out of phase (with a time delay) toward the end of the growing season compared to satellite LAI data and the GPP flux (Figure 6). The ground LAI (2D scans) corresponds to the green LAI. However, green parts of *Sphagnum*, especially when the latter has fully grown, may not see the light because they remain hidden in the shadow of the dense carpet of *Sphagnum*. The green LAI, therefore, corresponds to a measure of living, green biomass capable of photosynthesizing. However, for part of the green plant, no photosynthesis will occur because of the lack of light. The satellite LAI, therefore, seems to better fit with the leaf surface responsible for photosynthesis and not the total green surface of the plant. However, as explained by Weiss et al. (2020), the satellite-derived LAI is defined as an effective LAI not taking into account the clumping effect. Thus, as effective LAI is lower than true LAI, correcting the data by taking it into account could lead to higher values of satellite-derived *Sphagnum* LAI.

Satellite LAI values are most certainly underestimated. This type of measurement therefore, provides a low estimate of the range of *Sphagnum* peatlands LAI but reflect their seasonal evolution.

4.3. Seasonal Functioning of the Peatland in Response to Physical Drivers (Photosynthetic Active Radiations, Air Temperature and WTD) as Revealed by Vegetation Indices

At our site, the GCC values range from 0.3 to a little more than 0.5 for *Sphagnum* and 0.45 for herbaceous plants. They are in the high range of values reported by Linkosalmi et al. (2022) for three natural open peatlands although their study was not focused on *Sphagnum*. Since vegetation indices can be calculated using different wavelength ranges, it is sometimes possible to calculate the same vegetation index in different ways. This is the case for the CI index with the Sentinel-2 data. Clevers and Gitelson (2013) used band 7 of Sentinel-2, whereas we chose band 6, closer to the original definition of Gitelson and Merzlyak (1994). In our study, the values of the CI index are therefore lower than those reported by Clevers and Gitelson (2013), and in agreement with other studies (Clevers et al., 2017). The values of MSI and NDVI are also in agreement with the ranges reported in previous studies (Kolari et al., 2022; Meingast et al., 2014; Tucker et al., 2022).

We highlight a strong correlation between the annual cycles of midday GPP flux and CI, GCC, and LAI values ($R^2 = 0.94, 0.94, 0.83$) (Figure 6). These results are in line with previous works (Lees et al., 2020; Letendre et al., 2008; Street et al., 2007; Tucker et al., 2022), and highlight that CI, GCC, and LAI index are powerful indicators of ecosystem carbon assimilation. As already mentioned by Lees et al. (2020) and Tucker et al. (2022), the CI index does not differentiate vegetation types (*Sphagnum* and herbaceous). GCC, satellite-derived LAI, NDVI, and MSI on the other hand, are able to discriminate *Sphagnum*. Thus, GCC and LAI which track plant phenology combined with CI, seem to be promising for carrying out large-scale monitoring of *Sphagnum* vegetation dynamics (development and carbon assimilation). At our site seasonal cycle of *Sphagnum* GPP is indistinguishable from herbaceous one (see Figure S2 in Supporting Information S1), yet the *Sphagnum* satellite LAI is higher than satellite herbaceous LAI. Thus, the GPP/LAI ratio corresponds to photosynthetic activity and is lower in *Sphagnum* compared to herbaceous species. This smaller photosynthesis efficiency per vegetation area unit has already been described in the literature (Bengtsson et al., 2016; Juutinen et al., 2017; Waite & Sack, 2010). The GPP/LAI ($\sim \frac{CI}{LAI}$ or $\frac{CI}{GCC}$) ratio could also be used for *sphagnum* mapping, by filtering high values and combine it with MSI index.

We also showed that the seasonal cycles of GPP and LAI are not identical, despite being roughly similar. This is particularly visible during the 2019 drought episode (Figure S4 in Supporting Information S1). The LAI drops sharply in July, while the CI remains quite high, reinforcing the interest in studying their respective evolutions. Moreover, with regard to the annual cycle, LAI continues to increase during the summer and slowly decreases down to around 2 in December while GPP starts to decrease in July and drops to zero in December. This shows that plant phenology, expressed by the LAI (or GCC), is not the limiting factor and that *Sphagnum* ability to carry out photosynthesis is limited by other factors at the end of the season. As mentioned above, we can think of solar radiation, due to its decline, but we could also hypothesize that a physiological process limits photosynthesis. Recent studies (Hilty et al., 2021) effectively highlighted a maximum development size for plants, which once reached, would trigger mechanisms for downregulating growth and photosynthesis. Besides, at the beginning of the season and at the seasonal decline, the peatland water table is high (> -0.15 m). These conditions correspond respectively to low GPP values in March and October ($< 3 \mu\text{mol}\cdot\text{m}^{-2}\cdot\text{s}^{-1}$) (Figure 6). One hypothesis to consider is that *Sphagnum* moss photosynthetic capacities are limited under high water table conditions, due to the low diffusion of gasses, especially CO_2 in water. Low PAR values at the end of the growing season also limit GPP.

5. Conclusions and Prospects

We established that for a mountainous peatland in the Pyrenees, the LAI of *Sphagnum* mosses presents a strong annual cycle, peaking around 7–10 m²·m⁻² in early summer. This was observed with both destructive ground measurements and the processing of 5 years of Sentinel-2 images. We showed that the MSI derived from Sentinel-2 differentiates *Sphagnum* mosses from vascular plants on the Bernadouze site and can be of interest in the identification and mapping of *Sphagnum* peatlands. We also highlighted how the CI and GCC indices may describe the physiology and phenology of *Sphagnum*. Combined with the LAI, these indices give a good description of the dynamics of *Sphagnum* vegetation. The average seasonal cycles of CI, GCC, and LAI vegetation indices are strongly correlated with instantaneous midday GPP flux over the 5 years studied.

We, therefore, encourage the community to test and evaluate these different vegetation indices and LAI on other peatland sites. Besides, similar work with higher resolution satellite data (VEN μ S and PlanetScope satellite) could refine the results, and make it easier to distinguish areas dominated by *sphagnum* mosses, especially those with smaller surfaces. We also encourage the community to include these vegetation indices in GPP and respiration flux models, which often aim to determine peatland carbon budgets. Continental surface models would benefit from incorporating the representation of *sphagnum* mosses, their high LAI and the many implications that are related to them.

Finally, interannual variability should be studied to observe the response to some extremes (drought, heat wave). This would further allow by combining observation and modeling work to monitor the sustainability of the peatland ecosystem in the context of global change.

Data Availability Statement

Data are available at <https://doi.org/10.5281/zenodo.7554537> (Garisoain, 2023). To generate the LAI with the SL2P10 algorithm, the code available on the GitHub project <https://github.com/rfernand387/LEAF-Toolbox/wiki/FAQ> was used (Fernandes et al., 2021). The S2M data set is freely available on the AERIS data center on the following <https://doi.org/10.25326/37#v2020.2> (Vernay et al., 2023). The S2M data are provided by Météo-France—CNRS, CNRM, Centre d'Études de la Neige, through AERIS.

References

- Arroyo-Mora, J. P., Kalacska, M., Soffer, R., Ifimov, G., Leblanc, G., Schaaf, E. S., & Lucanus, O. (2018). Evaluation of phenospectral dynamics with Sentinel-2A using a bottom-up approach in a northern ombrotrophic peatland. *Remote Sensing of Environment*, 216, 544–560. <https://doi.org/10.1016/j.rse.2018.07.021>
- Asner, G. P., Scurlock, J. M. O., & Hicke, J. A. (2003). Global synthesis of leaf area index observations: Implications for ecological and remote sensing studies. *Global Ecology and Biogeography*, 12(3), 191–205. <https://doi.org/10.1046/j.1466-822X.2003.00026.x>
- Bao, K., Wang, G., Xing, W., & Shen, J. (2015). Accumulation of organic carbon over the past 200 years in alpine peatlands, northeast China. *Environmental Earth Sciences*, 73(11), 7489–7503. <https://doi.org/10.1007/s12665-014-3922-1>
- Bengtsson, F., Granath, G., & Rydin, H. (2016). Photosynthesis, growth, and decay traits in *Sphagnum*—A multispecies comparison. *Ecology and Evolution*, 6(10), 3325–3341. <https://doi.org/10.1002/ece3.2119>
- Bond-Lamberty, B., & Gower, S. T. (2007). Estimation of stand-level leaf area for boreal bryophytes. *Oecologia*, 151(4), 584–592. <https://doi.org/10.1007/s00442-006-0619-5>
- Brown, L. A., Fernandes, R., Djamaï, N., Meier, C., Gobron, N., Morris, H., et al. (2021). Validation of baseline and modified Sentinel-2 Level 2 Prototype Processor leaf area index retrievals over the United States. *ISPRS Journal of Photogrammetry and Remote Sensing*, 175, 71–87. <https://doi.org/10.1016/j.isprsjprs.2021.02.020>
- Chaudhary, N., Miller, P. A., & Smith, B. (2017). Modelling past, present and future peatland carbon accumulation across the pan-Arctic region. *Biogeosciences*, 14(18), 4023–4044. <https://doi.org/10.5194/bg-14-4023-2017>
- Chaudhary, N., Westermann, S., Lamba, S., Shurpali, N., Sannel, A. B. K., Schurgers, G., et al. (2020). Modelling past and future peatland carbon dynamics across the pan-Arctic. *Global Change Biology*, 26(7), 4119–4133. <https://doi.org/10.1111/gcb.15099>
- Chaudhary, N., Zhang, W., Lamba, S., & Westermann, S. (2022). Modeling pan-Arctic peatland carbon dynamics under alternative warming scenarios. *Geophysical Research Letters*, 49(10), e2021GL095276. <https://doi.org/10.1029/2021GL095276>
- Chen, J. M., & Black, T. A. (1992). Defining leaf area index for non-flat leaves. *Plant, Cell and Environment*, 15(4), 421–429. <https://doi.org/10.1111/j.1365-3040.1992.tb00992.x>
- Clevers, J. G. P. W., & Gitelson, A. A. (2013). Remote estimation of crop and grass chlorophyll and nitrogen content using red-edge bands on Sentinel-2 and -3. *International Journal of Applied Earth Observation and Geoinformation*, 23, 344–351. <https://doi.org/10.1016/j.jag.2012.10.008>
- Clevers, J. G. P. W., Kooistra, L., & Van den Brande, M. M. M. (2017). Using Sentinel-2 data for retrieving LAI and leaf and canopy chlorophyll content of a potato crop. *Remote Sensing*, 9(5), 405. <https://doi.org/10.3390/rs9050405>
- Clymo, R. S., & Hayward, P. M. (1982). The ecology of *Sphagnum*. In A. J. E. Smith (Ed.), *Bryophyte ecology* (pp. 229–289). Springer Netherlands. https://doi.org/10.1007/978-94-009-5891-3_8

Acknowledgments

R. Garisoain is funded by Meteo-France PhD Fellowship. This project was supported by Observatoire Homme Milieu Pyrenees Haut-Vicdessos, LABEX DRIHM (ANR-11-LBX-0010), and was undertaken in the framework of the Service National d'Observation Tourbières (SNO—French Peatland Observatory), part of the research infrastructure OZCAR, accredited by the INSU/CNRS. Additional support was provided by Observatoire Midi Pyrénées (OMP) and by the European Union's Horizon 2020 (H2020) research and innovation program under Grant Agreement No. 101003536 (ESM202-5-Earth System Models for the Future). The authors thank Stéphane Binet for sharing the water table depth data, Matthieu Lafaysse for his work and advice on the generation and use of the S2M data set, as well as Guylaine Canut-Rocafort and the GMEI team of Météo France for allowing us to use the laboratory equipment to perform the LAI scans and Dominique Carrer for his expertise in the field.

- Davidson, S. J., Goud, E. M., Malhotra, A., Estey, C. O., Korsah, P., & Strack, M. (2021). Linear disturbances shift boreal peatland plant communities toward earlier peak greenness. *Journal of Geophysical Research: Biogeosciences*, 126(8), e2021JG006403. <https://doi.org/10.1029/2021JG006403>
- Druel, A., Peylin, P., Krinner, G., Ciais, P., Viovy, N., Peregon, A., et al. (2017). Towards a more detailed representation of high-latitude vegetation in the global land surface model ORCHIDEE (ORC-HL-VEGv1.0). *Geoscientific Model Development*, 10(12), 4693–4722. <https://doi.org/10.5194/gmd-10-4693-2017>
- Erudel, T., Fabre, S., Houet, T., Mazier, F., & Briottet, X. (2017). Criteria comparison for classifying peatland vegetation types using in situ hyperspectral measurements. *Remote Sensing*, 9(7), 748. <https://doi.org/10.3390/rs9070748>
- Fernandes, R., Baret, F., Brown, L., Canisius, F., Dash, J., Djamai, N., et al. (2021). LEAF toolbox [Software]. GitHub. Retrieved from <https://github.com/rfernand387/LEAF-Toolbox/wiki/RAF>
- Ferretto, A., Brooker, R., Aitkenhead, M., Matthews, R., & Smith, P. (2019). Potential carbon loss from Scottish peatlands under climate change. *Regional Environmental Change*, 19(7), 2101–2111. <https://doi.org/10.1007/s10113-019-01550-3>
- Garisoain, R. (2023). Sentinel-2 derived *Sphagnum* and herbaceous CI, GCC, NDVI, MSI, SL2P10 LAI, and hourly temperature, water table depth, PAR on the Bernadouze peatland from 2017 to 2021 and 2D scans LAI over 2021 [Dataset]. Zenodo. <https://doi.org/10.5281/zenodo.7554537>
- Gascoin, S., & Fanise, P. (2018). Bernadouze meteorological data [Dataset]. SEDOOOMP. <https://doi.org/10.6096/DV/UQITZ4>
- Gitelson, A. A., & Merzlyak, M. N. (1994). Quantitative estimation of chlorophyll-*a* using reflectance spectra: Experiments with autumn chestnut and maple leaves. *Journal of Photochemistry and Photobiology B: Biology*, 22(3), 247–252. [https://doi.org/10.1016/1011-1344\(93\)06963-4](https://doi.org/10.1016/1011-1344(93)06963-4)
- Gitelson, A. A., Viña, A., Ciganda, V., Rundquist, D. C., & Arkebauer, T. J. (2005). Remote estimation of canopy chlorophyll content in crops. *Geophysical Research Letters*, 32(8), L08403. <https://doi.org/10.1029/2005GL022688>
- Harris, A. (2008). Spectral reflectance and photosynthetic properties of *Sphagnum* mosses exposed to progressive drought. *Ecohydrology*, 1(1), 35–42. <https://doi.org/10.1002/eco.5>
- Harris, A., Bryant, R. G., & Baird, A. J. (2006). Mapping the effects of water stress on *Sphagnum*: Preliminary observations using airborne remote sensing. *Remote Sensing of Environment*, 100(3), 363–378. <https://doi.org/10.1016/j.rse.2005.10.024>
- Hayward, P. M., & Clymo, R. S. (1983). The growth of *Sphagnum*: Experiments on, and simulation of, some effects of light flux and water-table depth. *Journal of Ecology*, 71(3), 845–863. <https://doi.org/10.2307/2259597>
- Henry, E., Infante Sanchez, M., & Corriol, G. (2014). *Tourbière de Bernadouze (Suc-et-Sentenac, 09). Expérimentation d'une cartographie fine des végétations (Technical Report)*. Conservatoire Botanique National des Pyrénées et de Midi-Pyrénées.
- Hilty, J., Muller, B., Pantin, F., & Leuzinger, S. (2021). Plant growth: The what, the how, and the why. *New Phytologist*, 232(1), 25–41. <https://doi.org/10.1111/nph.17610>
- Hugelius, G., Bockheim, J. G., Camill, P., Elberling, B., Grosse, G., Harden, J. W., et al. (2013). A new data set for estimating organic carbon storage to 3 m depth in soils of the northern circumpolar permafrost region. *Earth System Science Data*, 5(2), 393–402. <https://doi.org/10.5194/essd-5-393-2013>
- Jalut, G., Delibrias, G., Dagnac, J., Mardones, M., & Bouhours, M. (1982). A palaeoecological approach to the last 21 000 years in the Pyrenees: The peat bog of Freychinede (alt. 1350 m, Ariège, South France). *Palaeogeography, Palaeoclimatology, Palaeoecology*, 40(4), 321–359. [https://doi.org/10.1016/0031-0182\(82\)90033-5](https://doi.org/10.1016/0031-0182(82)90033-5)
- Janssens, I. A., Lankreijer, H., Matteucci, G., Kowalski, A. S., Buchmann, N., Epron, D., et al. (2001). Productivity overshadows temperature in determining soil and ecosystem respiration across European forests: Respiration across European forests. *Global Change Biology*, 7(3), 269–278. <https://doi.org/10.1046/j.1365-2486.2001.00412.x>
- Jonckheere, I., Fleck, S., Nackaerts, K., Muys, B., Coppin, P., Weiss, M., & Baret, F. (2004). Review of methods for in situ leaf area index determination: Part I. Theories, sensors and hemispherical photography. *Agricultural and Forest Meteorology*, 121(1), 19–35. <https://doi.org/10.1016/j.agrformet.2003.08.027>
- Joosten, H., & Clarke, D. (2002). In International Peat Society (Ed.), *Wise use of mires and peatlands*. International Mire Conservation Group.
- Joosten, H., Tanneberger, F., & Moen, A. (2017). *Mires and peatlands of Europe*. Schweizerbart'sche Verlagsbuchhandlung. Retrieved from https://www.schweizerbart.de/publications/detail/isbn/9783510653836/Joosten_Tann
- Juutinen, S., Virtanen, T., Kondratyev, V., Laurila, T., Linkosalmi, M., Mikola, J., et al. (2017). Spatial variation and seasonal dynamics of leaf-area index in the Arctic tundra-implications for linking ground observations and satellite images. *Environmental Research Letters*, 12(9), 095002. <https://doi.org/10.1088/1748-9326/aa7f85>
- Kganyago, M., Mhangara, P., Alexandridis, T., Laneve, G., Ovakoglou, G., & Mashiyi, N. (2020). Validation of Sentinel-2 leaf area index (LAI) product derived from SNAP toolbox and its comparison with global LAI products in an African semi-arid agricultural landscape. *Remote Sensing Letters*, 11(10), 883–892. <https://doi.org/10.1080/2150704X.2020.1767823>
- Kolari, T. H. M., Sallinen, A., Wolff, F., Kumpula, T., Tolonen, K., & Tahvanainen, T. (2022). Ongoing Fen–Bog transition in a boreal Aapa Mire inferred from repeated field sampling, aerial images, and Landsat data. *Ecosystems*, 25(5), 1166–1188. <https://doi.org/10.1007/s10021-021-00708-7>
- Korrensalo, A., Alekseychik, P., Hájek, T., Rinne, J., Vesala, T., Mehtätalo, L., et al. (2017). Species-specific temporal variation in photosynthesis as a moderator of peatland carbon sequestration. *Biogeosciences*, 14(2), 257–269. <https://doi.org/10.5194/bg-14-257-2017>
- Lees, K. J., Artz, R. R. E., Khomik, M., Clark, J. M., Ritson, J., Hancock, M. H., et al. (2020). Using spectral indices to estimate water content and GPP in *Sphagnum* moss and other peatland vegetation. *IEEE Transactions on Geoscience and Remote Sensing*, 58(7), 4547–4557. <https://doi.org/10.1109/TGRS.2019.2961479>
- Letendre, J., Poulin, M., & Rochefort, L. (2008). Sensitivity of spectral indices to CO₂ fluxes for several plant communities in a *Sphagnum*-dominated peatland. *Canadian Journal of Remote Sensing*, 34(sup 2), S414–S425. <https://doi.org/10.5589/m08-053>
- Linkosalmi, M., Tuovinen, J.-P., Nevalainen, O., Peltoniemi, M., Taniš, C. M., Arslan, A. N., et al. (2022). Tracking vegetation phenology of pristine northern boreal peatlands by combining digital photography with CO₂ flux and remote sensing data. *Biogeosciences*, 19(19), 4747–4765. <https://doi.org/10.5194/bg-19-4747-2022>
- Loisel, J., van Bellen, S., Pelletier, L., Talbot, J., Hugelius, G., Karran, D., et al. (2017). Insights and issues with estimating northern peatland carbon stocks and fluxes since the Last Glacial Maximum. *Earth-Science Reviews*, 165, 59–80. <https://doi.org/10.1016/j.earscirev.2016.12.001>
- Loisel, J., Yu, Z., Beilman, D. W., Camill, P., Alm, J., Amesbury, M. J., et al. (2014). A database and synthesis of northern peatland soil properties and Holocene carbon and nitrogen accumulation. *The Holocene*, 24(9), 1028–1042. <https://doi.org/10.1177/0959683614538073>
- Meingast, K. M., Falkowski, M. J., Kane, E. S., Potvin, L. R., Benscoter, B. W., Smith, A. M. S., et al. (2014). Spectral detection of near-surface moisture content and water-table position in northern peatland ecosystems. *Remote Sensing of Environment*, 152, 536–546. <https://doi.org/10.1016/j.rse.2014.07.014>
- Millar, D. J., Cooper, D. J., Dwire, K. A., Hubbard, R. M., & von Fischer, J. (2017). Mountain peatlands range from CO₂ sinks at high elevations to sources at low elevations: Implications for a changing climate. *Ecosystems*, 20(2), 416–432. <https://doi.org/10.1007/s10021-016-0034-7>

- Minasny, B., Berglund, O., Connolly, J., Hedley, C., de Vries, F., Gimona, A., et al. (2019). Digital mapping of peatlands—A critical review. *Earth-Science Reviews*, *196*, 102870. <https://doi.org/10.1016/j.earscirev.2019.05.014>
- Müller, J., & Joos, F. (2020). Global peatland area and carbon dynamics from the Last Glacial Maximum to the present—A process-based model investigation. *Biogeosciences*, *17*(21), 5285–5308. <https://doi.org/10.5194/bg-17-5285-2020>
- Niinemets, U., & Tobias, M. (2019). Canopy leaf area index at its higher end: Dissection of structural controls from leaf to canopy scales in bryophytes. *New Phytologist*, *223*(1), 118–133. <https://doi.org/10.1111/nph.15767>
- Pang, Y., Huang, Y., Zhou, Y., Xu, J., & Wu, Y. (2020). Identifying spectral features of characteristics of *Sphagnum* to assess the remote sensing potential of peatlands: A case study in China. *Mires & Peat*, *26*(25), 1–19. <https://doi.org/10.19189/MaP.2019.OMB.StA.1834>
- Potila, H., & Sarjala, T. (2004). Seasonal fluctuation in microbial biomass and activity along a natural nitrogen gradient in a drained peatland. *Soil Biology and Biochemistry*, *36*(7), 1047–1055. <https://doi.org/10.1016/j.soilbio.2004.02.014>
- Pullens, J. W. M., Sottocornola, M., Kiely, G., Toscano, P., & Gianelle, D. (2016). Carbon fluxes of an alpine peatland in Northern Italy. *Agricultural and Forest Meteorology*, *220*, 69–82. <https://doi.org/10.1016/j.agrformet.2016.01.012>
- Räsänen, A., Juutinen, S., Kalácska, M., Aurela, M., Heikkinen, P., Mäenpää, K., et al. (2020). Peatland leaf-area index and biomass estimation with ultra-high resolution remote sensing. *GIScience and Remote Sensing*, *57*(7), 943–964. <https://doi.org/10.1080/15481603.2020.1829377>
- Reille, M. (1990). The peat-bog of La Borde (eastern Pyrenees, France): A key site for the study of the Lateglacial in southern France. La tourbière de La Borde (Pyrenees orientales, France): un site de pour l'étude du Tardiglaciaire sud-européen. *Comptes Rendus de l'Académie des Sciences, Serie 2; (France)* (Vol. 310, p. 6). Retrieved from <https://www.osti.gov/etdweb/biblio/6693605>
- Richardson, A. D., Jenkins, J. P., Braswell, B. H., Hollinger, D. Y., Ollinger, S. V., & Smith, M.-L. (2007). Use of digital webcam images to track spring green-up in a deciduous broadleaf forest. *Oecologia*, *152*(2), 323–334. <https://doi.org/10.1007/s00442-006-0657-z>
- Riutta, T., Laine, J., Aurela, M., Rinne, J., Vesala, T., Laurila, T., et al. (2007). Spatial variation in plant community functions regulates carbon gas dynamics in a boreal fen ecosystem. *Tellus B: Chemical and Physical Meteorology*, *59*(5), 838–852. <https://doi.org/10.1111/j.1600-0889.2007.00302.x>
- Rosset, T., Binet, S., Antoine, J.-M., Lerigoleur, E., Rigal, F., & Gandois, L. (2020). Drivers of seasonal- and event-scale DOC dynamics at the outlet of mountainous peatlands revealed by high-frequency monitoring. *Biogeosciences*, *17*(13), 3705–3722. <https://doi.org/10.5194/bg-17-3705-2020>
- Rosset, T., Gandois, L., Le Roux, G., Teisserenc, R., Durantez Jimenez, P., Camboulive, T., & Binet, S. (2019). Peatland contribution to stream organic carbon exports from a montane watershed. *Journal of Geophysical Research: Biogeosciences*, *124*(11), 3448–3464. <https://doi.org/10.1029/2019JG005142>
- Rouse, J. W., Haas, R. H., Schell, J. A., & Deering, D. W. (1974). Monitoring vegetation systems in the Great Plains with ERTS. Retrieved from <https://ntrs.nasa.gov/citations/19740022614>
- Shi, X., Ricciuto, D. M., Thornton, P. E., Xu, X., Yuan, F., Norby, R. J., et al. (2021). Extending a land-surface model with *Sphagnum* moss to simulate responses of a northern temperate bog to whole ecosystem warming and elevated CO₂. *Biogeosciences*, *18*(2), 467–486. <https://doi.org/10.5194/bg-18-467-2021>
- Sonnenntag, O., Talbot, J., Chen, J. M., & Roulet, N. T. (2007). Using direct and indirect measurements of leaf area index to characterize the shrub canopy in an ombrotrophic peatland. *Agricultural and Forest Meteorology*, *144*(3), 200–212. <https://doi.org/10.1016/j.agrformet.2007.03.001>
- Street, L. E., Shaver, G. R., Williams, M., & Van Wijk, M. T. (2007). What is the relationship between changes in canopy leaf area and changes in photosynthetic CO₂ flux in arctic ecosystems? *Journal of Ecology*, *95*(1), 139–150. <https://doi.org/10.1111/j.1365-2745.2006.01187.x>
- Treat, C. C., Kleinen, T., Broothaerts, N., Dalton, A. S., Dommain, R., Douglas, T. A., et al. (2019). Widespread global peatland establishment and persistence over the last 130,000 y. *Proceedings of the National Academy of Sciences of the United States of America*, *116*(11), 4822–4827. <https://doi.org/10.1073/pnas.1813305116>
- Tucker, C., O'Neill, A., Meingast, K., Bourgeau-Chavez, L., Lilleskov, E., & Kane, E. S. (2022). Spectral indices of vegetation condition and soil water content reflect controls on CH₄ and CO₂ exchange in *Sphagnum*-dominated northern peatlands. *Journal of Geophysical Research: Biogeosciences*, *127*(7), e2021JG006486. <https://doi.org/10.1029/2021JG006486>
- van der Knaap, W. O., Lamentowicz, M., van Leeuwen, J. F. N., Hangartner, S., Leuenberger, M., Mauquoy, D., et al. (2011). A multi-proxy, high-resolution record of peatland development and its drivers during the last millennium from the subalpine Swiss Alps. *Quaternary Science Reviews*, *30*(23), 3467–3480. <https://doi.org/10.1016/j.quascirev.2011.06.017>
- Vernay, M., Lafaysse, M., & Hagenmuller, P. (2023). The S2M meteorological and snow cover reanalysis in the French mountainous areas (1958–present) [Dataset]. AERIS. <https://doi.org/10.25326/37#v2020.2>
- Vernay, M., Lafaysse, M., Monteiro, D., Hagenmuller, P., Nheili, R., Samacoïts, R., et al. (2022). The S2M meteorological and snow cover reanalysis over the French mountainous areas: Description and evaluation (1958–2021). *Earth System Science Data*, *14*(4), 1707–1733. <https://doi.org/10.5194/essd-14-1707-2022>
- Vogelmann, J. E., & Rock, B. N. (1986). Assessing forest decline in coniferous forests of Vermont using NS-001 Thematic Mapper Simulator data. *International Journal of Remote Sensing*, *7*(10), 1303–1321. <https://doi.org/10.1080/01431168608948932>
- Waite, M., & Sack, L. (2010). How does moss photosynthesis relate to leaf and canopy structure? Trait relationships for 10 Hawaiian species of contrasting light habitats. *New Phytologist*, *185*(1), 156–172. <https://doi.org/10.1111/j.1469-8137.2009.03061.x>
- Wania, R., Ross, I., & Prentice, I. C. (2009). Integrating peatlands and permafrost into a dynamic global vegetation model: 2. Evaluation and sensitivity of vegetation and carbon cycle processes. *Global Biogeochemical Cycles*, *23*(3), GB3014. <https://doi.org/10.1029/2008GB003413>
- Weiss, M., Baret, F., & Jay, S. (2020). ATBD—S2ToolBox Level 2 products: LAI, FAPAR, FCOVER (Technical Report No. Version 2.0). Retrieved from http://step.esa.int/docs/extra/ATBD_S2ToolBox_V2.0.pdf
- Williams, C. J., & Yavitt, J. B. (2003). Botanical composition of peat and degree of peat decomposition in three temperate peatlands. *Écoscience*, *10*(1), 85–95. <https://doi.org/10.1080/11956860.2003.11682755>
- Wilson, D., Alm, J., Riutta, T., Laine, J., Byrne, K. A., Farrell, E. P., & Tuittila, E.-S. (2007). A high resolution green area index for modelling the seasonal dynamics of CO₂ exchange in peatland vascular plant communities. *Plant Ecology*, *190*(1), 37–51. <https://doi.org/10.1007/s11258-006-9189-1>
- Xu, J., Morris, P. J., Liu, J., & Holden, J. (2018). PEATMAP: Refining estimates of global peatland distribution based on a meta-analysis. *Catena*, *160*, 134–140. <https://doi.org/10.1016/j.catena.2017.09.010>
- Yu, Z. C. (2012). Northern peatland carbon stocks and dynamics: A review. *Biogeosciences*, *9*(10), 4071–4085. <https://doi.org/10.5194/bg-9-4071-2012>
- Zhao, B., & Zhuang, Q. (2023). Peatlands and their carbon dynamics in northern high latitudes from 1990 to 2300: A process-based biogeochemistry model analysis. *Biogeosciences*, *20*(1), 251–270. <https://doi.org/10.5194/bg-20-251-2023>